14th International Conference on Structural Safety and Reliability - ICOSSAR'25
1-6 June, 2025 - Los Angeles California, USA
R. Ghanem, E. Johnson, S. Masri and A. Olivier (Eds)

SEQUENTIAL MULTIPLE IMPORTANCE SAMPLING FOR RELIABILITY ESTIMATION

WEILI XIA[1], ZIHAN LIAO[2] AND BINBIN LI [3]

[1] College of Civil Engineering and Architecture, Zhejiang University
Hangzhou, Zhejiang, China
12112070@zju.edu.cn

[2] College of Civil Engineering and Architecture, Zhejiang University
Hangzhou, Zhejiang, China
zihanliao@intl.zju.edu.cn

[3] State Key Laboratory of Biobased Transportation Fuel Technology, ZJU-UIUC Institute, Zhejiang University
Haining, Zhejiang, China
bbl@zju.edu.cn

Key words: Failure probability estimation; Bayesian inference; Multiple importance sampling; Subset simulation; Bias reduction.

Abstract. This study proposes a sequential multiple importance sampling (SeMIS) method for efficient estimation of rare event failure probability, which is typically represented by $p_f = \int_{\mathcal{F}} \phi_n(\boldsymbol{u})d\boldsymbol{u} = \int_{\mathbb{R}^n} \phi_n(\boldsymbol{u})\mathbb{I}_{\mathcal{F}}(\boldsymbol{u})d\boldsymbol{u}$. Regarding $\phi_n(\boldsymbol{u})$ as a prior distribution and $\mathbb{I}_{\mathcal{F}}(\boldsymbol{u})$ as the likelihood function, the failure probability p_f is equivalent to the evidence in Bayesian inference. Leveraged on this equivalence, the MIS used for Bayesian inference is adapted for failure probability estimation in this paper. In order to efficiently design the proposal distributions in MIS, we extend the idea of subset simulation (SuS) to adaptively define proposal distributions that propagate samples from both safe and failure domains to the limit state surface. In order to generate samples in the failure domain, an enlarged sampling parameter space is first designed by amplifying the standard deviation in "prior" distribution $\phi_n(\boldsymbol{u})$ from 1 to σ (≥ 1), i.e., to sample from $\phi_n(\sigma\boldsymbol{u})$. A heuristic rule to determine the optimal σ is proposed, which is inversely proportional to the dimension of the problem and converge to 1 when the dimension becomes large enough. The performance of SeMIS algorithm is illustrated in various benchmark examples and compared with SuS. It shows that SeMIS yields an excellent estimation of failure probability in terms of estimation bias and statistical/computational efficiency. It is also robust to the pathological geometry of the limit state function, where SuS may fail. The SeMIS algorithm provides a competitive solution for failure probability estimation.

1 INTRODUCTION

Structural reliability estimation plays a critical role in risk analysis and performance

evaluation in engineering field. This method facilitates a comprehensive probabilistic evaluation to quantify the extent to which engineered systems conform to prescribed safety and operational requirements. When examining distinct failure mechanisms, the associated failure probability p_f constitutes a critical probabilistic metric derived through a multidimensional integral [1]:

$$p_f = \int_{\Omega} \pi(\boldsymbol{x}) d\boldsymbol{x} = \int_{\mathbb{R}^n} \pi(\boldsymbol{x}) \mathbb{I}_{\Omega}(\boldsymbol{x}) d\boldsymbol{x} \tag{1}$$

where $\boldsymbol{X} = [X_1, X_2, \cdots, X_n]^{\mathrm{T}} \in \mathbb{R}^n$ denote an n-dimensional random vector characterizing uncertain parameters governing system behavior; $\pi(\boldsymbol{x})$ is the joint probability density function (PDF) of $\boldsymbol{X}$, which is typically derived from codified specifications in engineering practice or empirical data from observational studies; $\Omega = \{\boldsymbol{x} \in \mathbb{R}^n | g(\boldsymbol{x}) \leq 0\}$ is the failure domain, where $g(\boldsymbol{x})$ is the limit state function (LSF) and delineates the boundary between the failure and safe domains; $\mathbb{I}_{\Omega}(\boldsymbol{x})$ is an indicator function, returning 1 if $\boldsymbol{x} \in \Omega$ and 0 otherwise.

In structural reliability estimation, probabilistic coordinate transformation to the standard normal space offers computational advantages through a bijective mapping $\boldsymbol{U} = \boldsymbol{T}(\boldsymbol{X})$, where the original random vector $\boldsymbol{X}$ is transformed into an uncorrelated standard normal vector $\boldsymbol{U}$. The mapping can be achieved by the Rosenblatt transformation [2] or Nataf transformation [3]. Within the transformed coordinate, the failure probability is re-expressed by

$$p_f = \int_{\mathcal{F}} \phi_n(\boldsymbol{u}) d\boldsymbol{u} = \int_{\mathbb{R}^n} \phi_n(\boldsymbol{u}) \mathbb{I}_{\mathcal{F}}(\boldsymbol{u}) d\boldsymbol{u} \tag{2}$$

where $\phi_n(\boldsymbol{u}) = \prod_{i=1}^{n} \phi(u_i)$, and "$\phi(\cdot)$" is the univariate standard normal PDF. The transformed LSF $g(\boldsymbol{u}) = g(\boldsymbol{T}^{-1}(\boldsymbol{u}))$ defines the failure domain $\mathcal{F} = \{\boldsymbol{u} \in \mathbb{R}^n | g(\boldsymbol{u}) \leq 0\}$ in the standard normal space.

The high-dimensional nature of random vector $\boldsymbol{U}$ in practical engineering applications precludes the implementation of conventional numerical integration. Therefore, Monte Carlo simulation (MCS) has been established as one of the predominant methods, with subsequent methodological enhancements focusing on variance reduction through advanced techniques. Contemporary developments in this domain include but are not limited to: importance sampling (IS) [4–6], directional simulation [7–9], line sampling [10–12], and subset simulation (SuS) [13]. Among these techniques, SuS has garnered scholarly attention within reliability engineering communities, owing to its computational efficiency in addressing high dimensional and multiple design points problems.

While SuS demonstrates measurable computational advantages over direct MCS [14], its efficiency diminishes notably in low-dimensional problems. More significantly, persistent concerns exist regarding its probabilistic estimation accuracy, as evidenced by the study [15] showing that SuS may produce biased estimation without considering the geometry of the LSF. The sampling mechanism of SuS inherently follows the localized gradient descent orientation of LSF, which might not align with the global direction toward the design point.

A sequential multiple importance sampling (SeMIS) algorithm is proposed for failure probability estimation, leveraging on a Bayesian interpretation of failure probability. In defining the proposal distributions, we borrow the idea of SuS to propagate samples from both safe and failure domains to the limit state surface. This approach alleviates the limitation of SuS when the LSF has misleading gradients while optimizing exploration of the failure boundary

by focusing computational resources on critical regions where failure probability mass concentrates.

This paper is organized into four primary sections. A brief review of MIS is provided in Section 2. In Section 3, we present the general principle of the SeMIS algorithm. The performance of the SeMIS algorithm is illustrated in Section 4 via various benchmark examples.

2 MULTIPLE IMPORTANCE SAMPLING

MIS [16,17] is a technique in Bayesian inference for efficiently evidence evaluation by integrating multiple proposal distributions. By dynamically weighting the contribution of each proposal distribution, MIS simultaneously incorporates multiple proposal distributions during evidence estimation. Since the mathematical formula of failure probability estimation shown in Eqn. (2) bears a profound theoretical analogy to Bayesian evidence computation when reinterpreting $\phi_n(\boldsymbol{u})$ as a prior distribution and $\mathbb{I}_{\mathcal{F}}(\boldsymbol{u})$ as a likelihood function, the failure probability estimation is equivalent to the evidence estimation in Bayesian inference. Given a proposal distribution set $\{q_i(\boldsymbol{u})\}_{i=0}^{M}$, the failure probability integration using MIS can be derived as:

$$p_f = \sum_{i=0}^{M} \int \alpha_i(\boldsymbol{u}) \frac{\phi_n(\boldsymbol{u})\mathbb{I}_{\mathcal{F}}(\boldsymbol{u})}{q_i(\boldsymbol{u})} q_i(\boldsymbol{u}) \mathrm{d}\boldsymbol{u} \tag{3}$$

where $\alpha_i(\boldsymbol{u})$ is defined as the proposal weight, representing the weight between different proposal distributions. The validity of the above equation relies on $\alpha_i(\boldsymbol{u})$ satisfying the following condition:

$$\sum_{i=0}^{M} \alpha_i(\boldsymbol{u}) = 1 \text{, when } \phi_n(\boldsymbol{u})\mathbb{I}_{\mathcal{F}}(\boldsymbol{u}) \neq 0 \tag{4}$$

This condition leads to a critical corollary: wherever $\phi_n(\boldsymbol{u})\mathbb{I}_{\mathcal{F}}(\boldsymbol{u}) \neq 0$, at least one proposal distributions $q_i(\boldsymbol{u})$ in the set $\{q_i(\boldsymbol{u})\}_{i=0}^{M}$ must maintain positive density, thereby guaranteeing that the union of supports from all proposal distributions fully envelops the failure domain defined by $\phi_n(\boldsymbol{u})\mathbb{I}_{\mathcal{F}}(\boldsymbol{u})$. A valid proposal distribution set of MIS is shown in Figure 1(a) while the proposal distributions of SuS are illustrated in Figure 1(b) for comparison.

In this paper, the "balance heuristic" (a robust and widely adopted weighting function strategy in MIS) is utilized to define the proposal weight $\alpha_i(\boldsymbol{u})$. For a sample $\{\boldsymbol{u}_k^i\}_{k=1}^{N_i}$ generated from the proposal distribution $q_i(\boldsymbol{u})$, the weights are assigned as:

$$\alpha_i(\boldsymbol{u}_k^i) = \frac{N_i q_i(\boldsymbol{u}_k^i)}{\sum_{j=0}^{M} N_j q_j(\boldsymbol{u}_k^i)} \tag{5}$$

where N_i represents the sample size from i-th proposal distribution. The MIS estimator for the failure probability p_f is derived as:

$$\begin{aligned}\hat{p}_f &= \sum_{i=0}^{M} \frac{1}{N_i} \sum_{k=1}^{N_i} \left(\frac{N_i q_i(\boldsymbol{u}_k^i)}{\sum_{j=0}^{M} N_j q_j(\boldsymbol{u}_k^i)} \right) \frac{\phi_n(\boldsymbol{u}_k^i) \mathbb{I}_{\mathcal{F}}(\boldsymbol{u}_k^i)}{q_i(\boldsymbol{u}_k^i)} \\ &= \sum_{i=0}^{M} \sum_{k=1}^{N_i} \frac{\phi_n(\boldsymbol{u}_k^i) \mathbb{I}_{\mathcal{F}}(\boldsymbol{u}_k^i)}{\sum_{j=0}^{M} N_j q_j(\boldsymbol{u}_k^i)} \\ &= \frac{1}{N_{all}} \sum_{i=0}^{M} \sum_{k=1}^{N_i} \frac{\phi_n(\boldsymbol{u}_k^i) \mathbb{I}_{\mathcal{F}}(\boldsymbol{u}_k^i)}{\sum_{j=0}^{M} c_j q_j(\boldsymbol{u}_k^i)}\end{aligned} \tag{6}$$

where $N_{all} = \sum_j N_j$ is the total number of samples, and $c_j = \frac{N_j}{N_{all}}$ is the fraction of samples from $q_j(\boldsymbol{u})$.

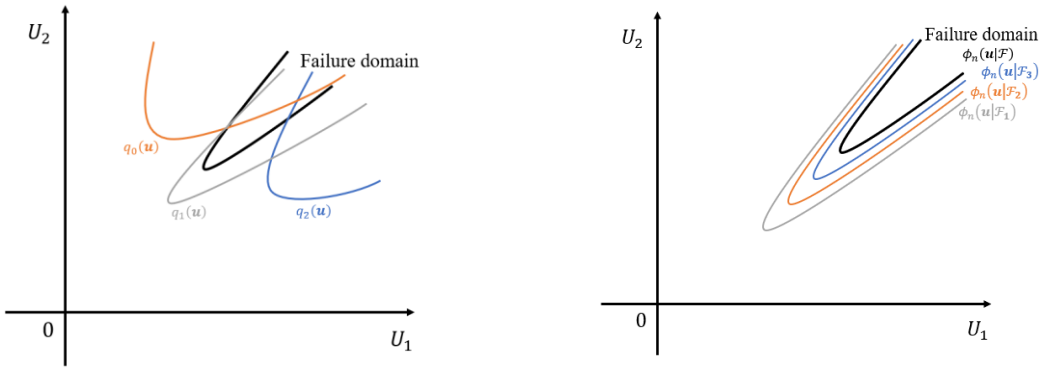

(a) MIS (b) SuS

Figure 1: Proposal distributions in SeMIS and SuS

3 SEQUENTIAL MULTIPLE IMPORTANCE SAMPLING

Realizing that MIS for failure probability estimation fundamentally increases the flexibility in proposal distribution determination. Borrowing the idea from SuS, we develop a sequential MIS (SeMIS) algorithm that simultaneously propagates samples from both safe and failure domain toward the limit state surface.

3.1 Initial distribution enlargement

The proposed methodology initiates with reconfiguration of the initial sampling distribution. In structural reliability analysis, the failure domain often lies in distant regions from the origin, where the PDF value of the initial distribution is relatively low. Consequently, adopting the standard normal distribution as the initial sampling distribution is generally inefficient to explore the failure domain. To facilitate more effective sampling in these low-probability regions, we deliberately enlarge the standard deviation in $\phi_n(\boldsymbol{u})$ from 1 to σ, thereby redefining the initial distribution as $\phi_n(\sigma\boldsymbol{u})$.

The calibration of the standard deviation amplification factor σ necessitates theoretical analysis. Consider an amplified random variable defined as $\boldsymbol{u}' = f(\boldsymbol{u}) = \sigma\boldsymbol{u}$. Based on the change-of-variable technique, the transformed PDF for the new random variable $\boldsymbol{u}'$ becomes:

$$p_{u'}(\boldsymbol{u}') = p_{\boldsymbol{u}}(f^{-1}(\boldsymbol{u}')) \cdot \left|\det\left[\boldsymbol{J}_{f^{-1}}(\boldsymbol{u}')\right]\right| = \phi_n\left(\frac{\boldsymbol{u}'}{\sigma}\right) \cdot \frac{1}{|\sigma|^n} \tag{7}$$

where $\det\left[\boldsymbol{J}_{f^{-1}}(\boldsymbol{u}')\right]$ denotes the Jacobian determinant quantifying the volume scaling rate between original and transformed coordinate systems. Note that this rate of volume change has a power relationship to dimension n. To ensure dimensionally invariant enlargement of probability volumes in SeMIS, the amplification factor σ is defined through the geometric relationship:

$$\sigma = \sqrt[n]{\beta} \tag{8}$$

where β ($\beta > 1$) is the probabilistic volume scaling ratio between the enlarged initial distribution of $\boldsymbol{u}'$ and the nominal distribution of $\boldsymbol{u}$. Through empirical investigations across various examples with multidimensional LSF, β is ultimately selected as 6, a value demonstrating robust performance in diverse examples. The asymptotic convergence of the amplification factor $\lim_{n\to\infty} \sigma = 1$ under increasing dimensionality reflects the Gaussian measure concentration in high-dimensional spaces. As n grows, Euclidean norms $\|\boldsymbol{u}\|_2$ concentrate near $\sqrt{n}$, rendering large amplification factor ($\sigma \gg 1$) counterproductive by displacing samples from high PDF regions. Note that when $\sigma = 1$, the initial distribution reduces precisely to the original standard normal distribution, and this configuration of the amplification factor σ maintains the algorithm's robustness against the high-dimensional measure concentration phenomenon.

The efficacy of initial distribution enlargement in two-dimensional space is demonstrated in Figure 2, where $\sigma = \sqrt[2]{6}$. It can be observed that in the two-dimensional case, enlarging the initial distribution allows a portion of the samples to fall within the failure domain at the outset, which can accelerate the exploration of the failure domain.

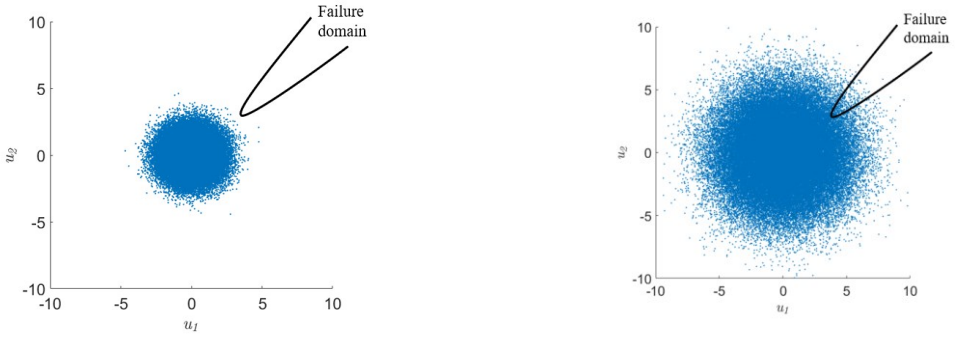

(a) Initial distribution of $\boldsymbol{u}$

(b) Initial distribution of $\boldsymbol{u}'$

Figure 2: Initial distribution enlargement in two-dimensional space

3.2 Bidirectional shrinkage

As established in the preceding discussion, the enlarged initial distribution significantly enhances failure domain penetration probability through amplifying standard deviation. Crucially, the enlarged initial distribution maintains strictly positive density in the whole failure domain ($p_{\boldsymbol{u}'}(\boldsymbol{u}') > 0$ when $\phi_n(\boldsymbol{u}')\mathbb{I}_{\mathcal{F}}(\boldsymbol{u}') \neq 0$), thereby satisfying the requirement in MIS.

This ensures all subsequent proposal distributions, regardless of their parametric forms, maintain MIS theoretical correctness throughout iterations.

Since the probability density of Gaussian distribution decays exponentially with the Euclidean norm to the origin, the probability mass of failure distribution concentrates near the limit state surface. This geometric property motivated the development of a bidirectional sampling strategy that synergistically utilizes samples from both safe and failure domains to shrink to the limit state surface by defining the proposal distributions as:

$$q_i(\boldsymbol{u}') = \frac{p_{\boldsymbol{u}'}(\boldsymbol{u}')\mathbb{I}(|g(\boldsymbol{u}')| \le l_i)}{p_i} \tag{9}$$

where $|\cdot|$ denotes the absolute value, p_i is the normalizing constant of the proposal distribution. The threshold sequence $\{l_i\}_{i=1}^{M}$ constitutes a monotonically decreasing absolute value of LSF, adaptively determined through probabilistic conditioning according to the target "level probability" p_0. In contrast to conventional SuS, this proposal distribution $q_i(\boldsymbol{u}')$ adjustment fundamentally alters the convergence orientation, shifting from unidirectional propagation toward the failure domain to targeted shrinkage to the limit state surface. This reorientation enables concentrated sampling in critical regions that have the most significantly impact on failure probability estimation. Figure 3 demonstrates the difference in proposal distribution geometry between SeMIS and SuS in a two-dimensional space. Notably, the proposal distributions of SeMIS framework shown as annular distributions concentrically enveloping the limit state surface.

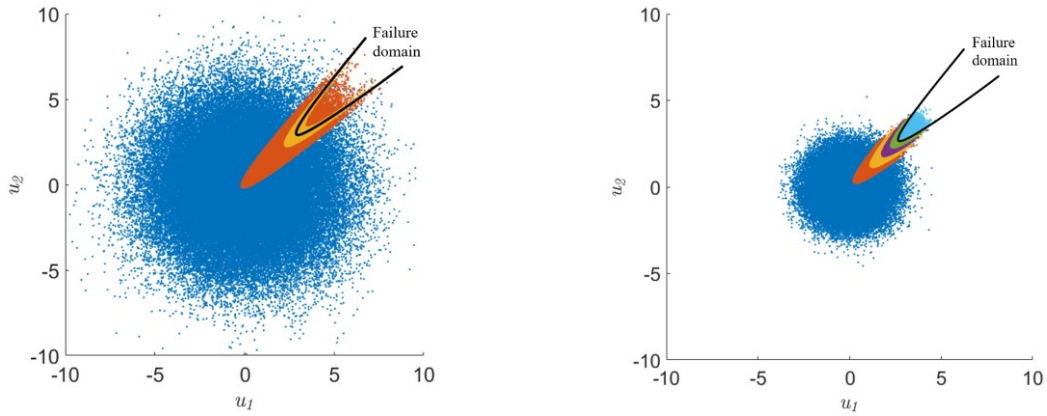

(a) SeMIS (b) SuS

Figure 3: Sample distribution convergency in two-dimensional space

SeMIS fundamentally diverges from SuS through two synergistic innovations: (1) strategic enlargement of the initial distribution via amplifying standard deviation, and (2) bidirectional exploration of the limit state surface. This dual mechanism not only accelerates probability mass concentration in critical failure regions, but also circumvents pathological bias induced by misleading gradient of LSF. To illustrate the advantage of SeMIS, we consider an example from Ref. [15]. Given a two-dimensional LSF $g(X_1, X_2)$ with misleading gradient in Eqn. (10) as a combination of piecewise linear functions, whose surface is spliced by multiple linear planes:

$$g(X_1, X_2) = \min(g_1, g_2) \tag{10}$$

where

$$\begin{aligned} g_1(X_1, X_2) &= \begin{cases} 4 - X_1 & , X_1 > 3.5 \\ 0.85 - 0.1X_1 & , X_1 \leq 3.5 \end{cases} \\ g_2(X_1, X_2) &= \begin{cases} 0.5 - 0.1X_2 & , X_2 > 2 \\ 2.3 - X_2 & , X_2 \leq 2 \end{cases} \end{aligned} \tag{11}$$

Here, both X_1 and X_2 follow the standard normal distribution.

The LSF $g(X_1, X_2)$ is illustrated in Figure 4(a), where the blue horizontal plane delineates the zero LSF, separating the safe and failure domains. Figure 4(b) presents the corresponding LSF contour plot. A purple arrow points towards the design point located at coordinates (4,0), while a red arrow denotes the direction aligned with the steepest descent gradient of the LSF near the origin.

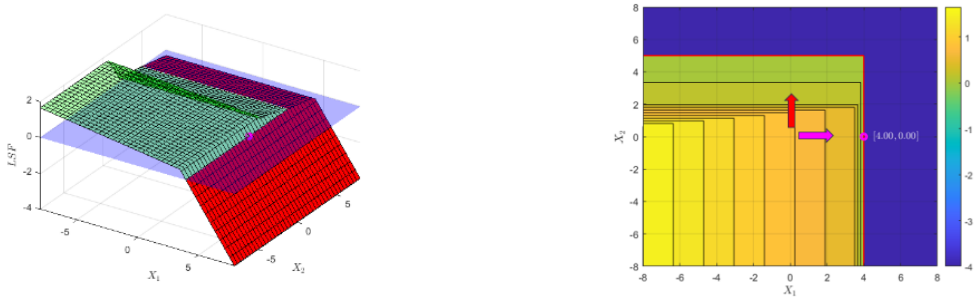

(a) 3D Geometry of LSF (b) Contour of LSF

Figure 4: The contour map of piecewise linear LSF

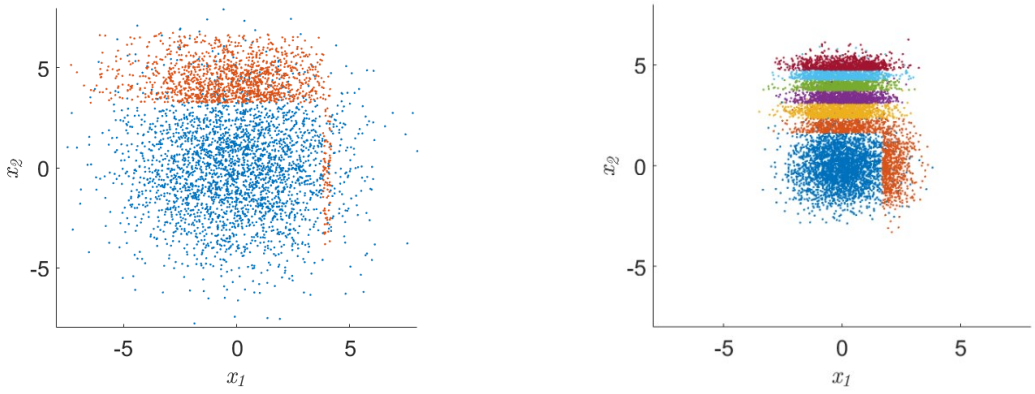

(a) SeMIS (b) SuS

Figure 5: Sample path generated by SeMIS and SuS

As demonstrated in Figure 5, The sample paths generated by SeMIS and original SuS show the progression of iterations of these two algorithms. In original SuS, samples exhibit migration

trajectories aligned with the steepest gradient descent direction toward the line of $x_2 = 5$, which unfortunately coincides with a low probability mass region within the failure domain. Conversely, SeMIS's enlarged initial distribution facilitates exploratory sampling across disjoint failure subdomains, enabling consistent convergence to the correct design point located at $(4,0)$. Despite fewer sample generated near the design point caused by non-uniform LSF gradient topology, SeMIS's design point exploration capability ensures estimator unbiasedness.

The capability to accurately identify the design point stems from the enlargement of initial distribution. Furthermore, as illustrated in Figure 5, SeMIS requires fewer iterations than original SuS when addressing the same problem, resulting in reduced computational effort and enhanced efficiency. This improvement arises from both the enlarged initial distribution and the bidirectional shrinkage mechanism of proposal distributions toward critical regions of the failure domain with high probability mass.

4 EMPIRICAL STUDIES

The proposed SeMIS algorithm is validated through three two-dimensional pathological problems derived from Ref. [15] and one benign benchmark problem with various dimensions. For completeness, both analytical expressions of the LSFs and corresponding graphical representations of the pathological problems are provided for visualization. Within the contour maps, the purple arrow identifies the gradient path toward the design point (denoted by a purple dot), whereas the red arrow highlights the principal orientation detected by the original SuS.

Example 1: Piecewise linear LSF

We first consider the problem mentioned in Section 3.3. The LSF $g(X_1, X_2)$ is given by Eqs.(10) and (11). As illustrated in Section 3.3, the gradient of the LSF guided samples to deviate from the right path towards to the design point.

Example 2: Changing Topological LSF

The next example is with changing topological structure of failure domains, where the LSF $g(X_1, X_2)$ is given by a simple metaball function:

$$g(X_1, X_2) = \frac{30}{\left(\frac{4(X_1+2)^2}{9} + \frac{X_2^2}{25}\right)^2 + 1} + \frac{20}{\left(\frac{(X_1-2.5)^2}{4} + \frac{(X_2-0.5)^2}{25}\right)^2 + 1} - 5 \tag{12}$$

To elucidate this example more effectively, the shape of the LSF function is plotted in Figure 6. One can envision the geometry of the LSF as resembling two mountain peaks. Due to the block of high peaks, most samples in the original SuS tends to propagate along the valley (highlighted by the red arrow), thus fail in capturing the design point.

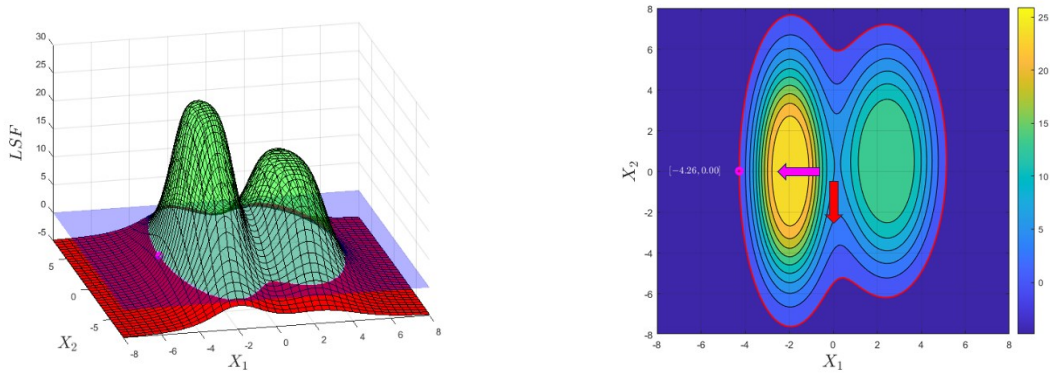

Figure 6: Changing Topological LSF and the contour map

Example 3: Linear Log LSF

The third example involves a LSF incorporating two functions: a linear function and a logistic function. The LSF is expressed as

$$g(X_1, X_2) = \min\left\{5 - X_1, \frac{1}{1+\exp\left(-2(X_2+4)\right)} - 0.5\right\} \tag{13}$$

As shown in Figure 7, this example bears resemblance to Example 1, as the LSFs in both cases exhibit misleading gradient near the origin.

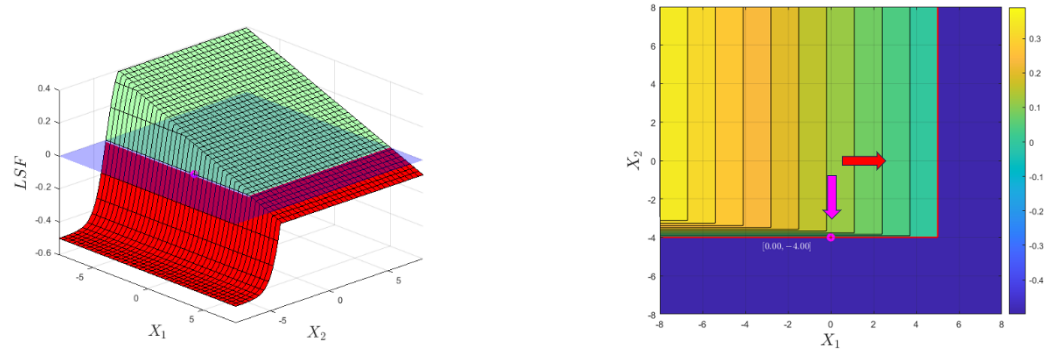

Figure 7: Linear Log LSF and the contour map

Example 4: High-dimensional nonlinear LSF

The fourth example is a benign problem taken from Ref. [18] where original SuS yields unbiased estimation result. It features with a high dimensional nonlinear LSF:

$$g(\boldsymbol{X}) = 4 - \frac{1}{\sqrt{n}}\sum_{i=1}^{n} X_i + \frac{5}{2}(X_1 - X_2)^2 \tag{14}$$

where X_i $(i = 1,2\cdots n)$ follows independent standard normal distribution and the failure probability $p_f = 4.29 \times 10^{-6}$, which remains invariant with respect to the dimension.

A comparative analysis of the proposed SeMIS and original SuS is conducted across all four problems. Both methodologies employed identical initial parameters, including a per-level sample size of $N = 1000$ and the level probability $p_0 = 0.1$, with the number of LSF evaluations tracked as an index for computational costs. For a thorough comparison, 100 independent runs are performed for each algorithm, enabling comprehensive performance benchmarking.

Table 1: Estimation results using SeMIS and SuS

Example	Reference p_f^*	n	SeMIS		SuS	
			$\tilde{p}_f/p_f^*$	# LSF ($\times 10^3$)	$\hat{p}_f/p_f^*$	# LSF ($\times 10^3$)
1	3.20×10^{-5}	2	1.01 ± 0.29	2.00	0.95 ± 1.33	5.87
2	1.13×10^{-5}	2	1.01 ± 0.26	2.00	1.19 ± 3.34	7.67
3	3.23×10^{-5}	2	1.00 ± 0.19	2.00	1.20 ± 4.02	6.59
4	4.29×10^{-6}	2	1.12 ± 0.34	2.96	1.16 ± 0.60	5.95
		5	1.12 ± 0.47	4.00	1.13 ± 0.67	5.94
		10	1.13 ± 0.58	4.92	1.14 ± 0.66	5.95
		20	1.12 ± 0.62	5.17	1.13 ± 0.70	5.94
		50	1.13 ± 0.69	5.73	1.20 ± 0.69	5.93
		100	1.15 ± 0.70	5.87	1.17 ± 0.63	5.94

The comparative results across all four problems are synthesized in Table 1. The reference failure probabilities are calculated via crude MCS with a sample size of 10^9. The estimation of SeMIS and SuS are shown as sample mean $\pm$ sample standard deviation, derived from 100 independent runs and normalized against reference values.

Notably, SuS exhibits larger estimation uncertainty (quantified by larger sample standard deviation) in pathological reliability problems (Example 1-3). This arises from divergent algorithmic convergence behaviors: some of runs successfully identifies design points, while others fail. The proposed SeMIS demonstrates superior statistical properties, exhibiting significantly reduced bias and deviation compared to SuS, while concurrently enhancing computational efficiency in these pathological problems. Quantitative validation across three case studies reveals deviation reductions of 78.2%, 92.2%, and 95.3% relative to SuS. The total of 2000 LSF evaluations, corresponding to just two iterations, reflects SeMIS's accelerated convergence. The enhanced computational efficiency originates from SeMIS's bidirectional exploration strategy and initial distribution enlargement. Through these two advancements, SeMIS bypasses the area with misleading gradient and directly locates the limit state surface near design point.

The SeMIS algorithm demonstrates statistically reductions in estimation bias compared to original SuS across all dimensional configurations when applied to benign problem (Example 4). However, the estimated standard deviation reduction advantage of SeMIS relative to SuS diminishes asymptotically with dimension growth. This phenomenon may stem from the exponential decay in the volume of the failure domain relative to the entire parameter space with increasing dimension. When the dimension exceeds critical thresholds and the amplification factor $\sigma \to 1$, SeMIS's performance becomes asymptotically comparable to

original SuS in terms of estimated standard deviation.

5 CONCLUSIONS

This study proposed a sequential multiple importance sampling (SeMIS) algorithm for rare event probability estimation in structural reliability. By reinterpreting the failure probability as the Bayesian evidence, SeMIS integrates multiple proposal distributions to estimate failure probability. The proposal distributions are adaptively constructed to synergistically propagate samples from safe and failure domains toward critical regions where failure probability mass concentrates. With two key advancements (initial distribution enlargement and bidirectional shrinkage), SeMIS demonstrates excellent estimation of failure probability in terms of estimation bias and statistical/computational efficiency through investigations on various examples.

REFERENCES

[1] A. Der Kiureghian, Structural and System Reliability, 1st ed., Cambridge University Press, 2022. https://doi.org/10.1017/9781108991889.

[2] M. Hohenbichler, R. Rackwitz, Non-Normal Dependent Vectors in Structural Safety, Journal of the Engineering Mechanics Division 107 (1981) 1227–1238. https://doi.org/10.1061/JMCEA3.0002777.

[3] P.-L. Liu, A. Der Kiureghian, Multivariate distribution models with prescribed marginals and covariances, Probabilistic Engineering Mechanics 1 (1986) 105–112. https://doi.org/10.1016/0266-8920(86)90033-0.

[4] S. Engelund, R. Rackwitz, A benchmark study on importance sampling techniques in structural reliability, Structural Safety 12 (1993) 255–276. https://doi.org/10.1016/0167-4730(93)90056-7.

[5] R.E. Melchers, Importance sampling in structural systems, Structural Safety 6 (1989) 3–10. https://doi.org/10.1016/0167-4730(89)90003-9.

[6] S.T. Tokdar, R.E. Kass, Importance sampling: a review, Wiley Interdisciplinary Reviews: Computational Statistics 2 (2010) 54–60.

[7] R.E. Melchers, Structural system reliability assessment using directional simulation, Structural Safety 16 (1994) 23–37. https://doi.org/10.1016/0167-4730(94)00026-M.

[8] M.A. Shayanfar, M.A. Barkhordari, M. Barkhori, M. Barkhori, An adaptive directional importance sampling method for structural reliability analysis, Structural Safety 70 (2018) 14–20. https://doi.org/10.1016/j.strusafe.2017.07.006.

[9] P. Bjerager, Probability Integration by Directional Simulation, Journal of Engineering Mechanics 114 (1988) 1285–1302. https://doi.org/10.1061/(ASCE)0733-9399(1988)114:8(1285).

[10] H.J. Pradlwarter, G.I. Schuëller, P.S. Koutsourelakis, D.C. Charmpis, Application of line sampling simulation method to reliability benchmark problems, Structural Safety 29 (2007) 208–221. https://doi.org/10.1016/j.strusafe.2006.07.009.

[11] J. Song, P. Wei, M. Valdebenito, M. Beer, Active learning line sampling for rare event analysis, Mechanical Systems and Signal Processing 147 (2021) 107113. https://doi.org/10.1016/j.ymssp.2020.107113.

[12] Z. Lu, S. Song, Z. Yue, J. Wang, Reliability sensitivity method by line sampling, Structural Safety 30 (2008) 517–532. https://doi.org/10.1016/j.strusafe.2007.10.001.
[13] S.-K. Au, J.L. Beck, Estimation of small failure probabilities in high dimensions by subset simulation, Probabilistic Engineering Mechanics 16 (2001) 263–277. https://doi.org/10.1016/S0266-8920(01)00019-4.
[14] S. Au, Y. Wang, Engineering Risk Assessment with Subset Simulation, 1st ed., Wiley, 2014. https://doi.org/10.1002/9781118398050.
[15] K. Breitung, The geometry of limit state function graphs and subset simulation: Counterexamples, Reliability Engineering & System Safety 182 (2019) 98–106. https://doi.org/10.1016/j.ress.2018.10.008.
[16] E. Veach, L.J. Guibas, Optimally combining sampling techniques for Monte Carlo rendering, in: Proceedings of the 22nd Annual Conference on Computer Graphics and Interactive Techniques - SIGGRAPH '95, ACM Press, Not Known, 1995: pp. 419–428. https://doi.org/10.1145/218380.218498.
[17] I. Kondapaneni, P. Vevoda, P. Grittmann, T. Skřivan, P. Slusallek, J. Křivánek, Optimal multiple importance sampling, ACM Trans. Graph. 38 (2019) 1–14. https://doi.org/10.1145/3306346.3323009.
[18] M. Ghalehnovi, M. Rashki, A. Ameryan, First order control variates algorithm for reliability analysis of engineering structures, Applied Mathematical Modelling 77 (2020) 829–847. https://doi.org/10.1016/j.apm.2019.07.049.